X-ray radiographic expansion measurements of isochorically heated thin wire targets

D. C. Hochhaus, B. Aurand, M. Basko, B. Ecker, T. Kühl et al.

Citation: Phys. Plasmas **20**, 062703 (2013); doi: 10.1063/1.4810801
View online: http://dx.doi.org/10.1063/1.4810801
View Table of Contents: http://pop.aip.org/resource/1/PHPAEN/v20/i6
Published by the AIP Publishing LLC.

X-ray radiographic expansion measurements of isochorically heated thin wire targets

D. C. Hochhaus,[1,2,3] B. Aurand,[1,4,3] M. Basko,[1,5] B. Ecker,[4,6,3] T. Kühl,[7,4,6,1] T. Ma,[8] F. Rosmej,[9,10] B. Zielbauer,[7,6] and P. Neumayer[1,3,a)]
[1]*ExtreMe Matter Institute EMMI, GSI, 64291 Darmstadt, Germany*
[2]*Goethe-Universität, 60438 Frankfurt am Main, Germany*
[3]*Frankfurt Institute for Advanced Studies, 60438 Frankfurt am Main, Germany*
[4]*Johannes Gutenberg-Universität, 55099 Mainz, Germany*
[5]*Alikhanov Institute for Theoretical and Experimental Physics, 117218 Moscow, Russia*
[6]*Helmholtz-Institut Jena, 07743 Jena, Germany*
[7]*GSI Helmholtzzentrum für Schwerionenforschung GmbH, 64291 Darmstadt, Germany*
[8]*Lawrence Livermore National Laboratory, Livermore, California 94550, USA*
[9]*UPMC, UMR7605, LULI, case 128, 4 Place Jussieu, 75252 Paris Cedex 05, France*
[10]*Ecole Polytechnique, LULI, PAPD, Route de Saclay, 91128 Palaiseau Cedex, France*

(Received 4 March 2013; accepted 7 May 2013; published online 19 June 2013)

Solid density matter at temperatures ranging from 150 eV to <5 eV has been created by irradiating thin wire targets with high-energy laser pulses at intensities $\approx 10^{18}$ W/cm^2. Energy deposition and transport of the laser-produced fast electrons are inferred from spatially resolved K_α-spectroscopy. Time resolved x-ray radiography is employed to image the target mass density up to solid density and proves isochoric heating. The subsequent hydrodynamic evolution of the target is observed for up to 3 ns and is compared to radiation-hydrodynamic simulations. At distances of several hundred micrometers from the laser interaction region, where temperatures of 5–20 eV and small temperature gradients are found, the hydrodynamic evolution of the wire is a near axially symmetric isentropic expansion, and good agreement between simulations and radiography data confirms heating of the wire over hundreds of micrometers. © *2013 AIP Publishing LLC*. [http://dx.doi.org/10.1063/1.4810801]

I. INTRODUCTION

Matter at high-energy densities (HED) can be found in compact astrophysical objects or at various stages of inertial confinement fusion, and knowledge of material properties such as the equation-of-state (EOS) is necessary for modeling these scenarios.[1,2] In particular, the regime of Warm Dense Matter (WDM), characterized by strong ion-ion coupling and partial electron degeneracy, poses a great challenge to current theory.[3,4] Powerful drivers, such as pulsed power generators, intense ion-beam accelerators, and high-energy laser facilities enable generation of HED matter in the laboratory for experiments that can provide stringent tests to dense matter modeling.

Rapid volumetric heating offers an interesting alternative to the well-established method of shock heating[5,6] for the generation of large, homogenous samples at WDM conditions. Provided the heating time is short compared to hydrodynamic timescales ("isochoric heating"), the initial mass density is well known. The subsequent isentropic expansion allows to access a wide parameter space. Intense short pulses of energetic particles created in the interaction of laser light at relativistic intensities with matter provide an excellent tool for such rapid heating. Laser-accelerated proton beams have been employed to heat solid aluminum foils to temperatures of 10's of eV,[7,8] where the final target temperature was inferred from thermal emission.

Interaction of laser light at relativistic intensities with matter has long been known to produce copious amounts of energetic electrons at mean kinetic energies of order 100s of keV to MeV. The conversion of laser energy into this "hot" electron fraction is very efficient, values of order several 10s percent having been reported (e.g., Ref. 9). The collisional stopping length of the energetic electrons in matter at solid density is of order millimeter. While this allows for a homogenous heating, the energy is deposited over large volumes. However, when using targets with dimensions much smaller than the average electron range the target rapidly charges up and strong electrostatic fields prevent the hot electrons from escaping the target.[10] The subsequent "refluxing" of the hot electrons through the target leads, e.g., to an increased x-ray yield.[11,12] Exploiting the confinement of refluxing hot electrons to the target volume, efficient heating of targets with reduced dimensions to temperatures exceeding 100 eV has been reported by numerous authors (e.g., Refs. 13–15).

In these previous experiments, isochoric heating was usually assumed. Time-resolved measurements of the target fluorescence show that the relaxation of hot electrons is on the time-scale of picoseconds,[16] and imaging of the fluorescence emission shows that the target remains in its initial dimensions during this relaxation process (e.g., Refs. 15 and 17). Measurements of the target hydrodynamic evolution subsequent to the heating were restricted to the expansion of underdense plasma by interferometric methods using optical probes (e.g., Refs. 7 and 18).

a)p.neumayer@gsi.de

In this paper, we report on experiments where we employ intense-laser generated hot electrons to heat matter along a wire up to distances of several hundred micrometers. Here, the material is unperturbed by the complex processes close to the laser-matter interaction region, e.g., radiative heating by the hot blow-off plasma or shock waves driven into the material. The heating process can thus be regarded as being purely caused by the energetic electrons originating hundreds of μm away. We confirmed the isochoric heating by employing x-ray radiography to image the target mass density up to solid density over time-scales long compared to the heating time. X-ray radiography also enables us to follow the isentropic expansion of the generated HED matter.

II. EXPERIMENT

The experiments were conducted at the PHELIX laser facility[19] at the GSI Helmholtzzentrum für Schwerionenforschung GmbH in Darmstadt, Germany. Fig. 1 shows a schematic of the experimental setup. Laser pulses of approximately 40 J and 8 ps duration were focused at an incidence angle of 35° onto the tip of free-standing titanium wires (diameter 50 μm, >5 mm length). The laser focal spot size was measured to be 20×30 μm, producing peak intensities of $\approx 10^{18}$ W/cm^2. The intensity contrast of the laser pulses was measured to be better than 10^6. The targets were fabricated from commercial titanium wire, which was embedded in a polymer resin, then cut perpendicular to the wire axis and the end face polished in order to provide a well defined flat surface for the interaction with the laser pulse. Finally, the resin was dissolved and the wires individually mounted on a target stalk (see inset in Fig. 1). The amount of laser light missing the target was measured by means of a scattering screen behind the target imaged onto an absolutely calibrated CCD-camera and was typically of order few percent. A second laser pulse ("backlighter," 50 J, 8 ps) was focused onto a thin (<10 μm) copper foil positioned below the wire target to provide an intense short x-ray source for radiographic images of the expanding wire. The intense-laser produced hot electrons generate K-shell fluorescence and bremsstrahlung within the backlighter target, and the duration of this emission is closely linked to the relaxation time-scale of the hot electrons, which is typically less than 10 ps.[16] This time-scale is short compared to the hydrodynamic time-scale for the expansion of the backlighter target and consequently the backlighter emission is spatially confined to the initial target dimensions. Thus, by viewing the backlighter foil edge-on, a small source size can be realized[20] as required for point-projection imaging of the thin wires. Spatially extended long-lasting thermal emission from Helium-like Cu-ions in the blow-off plasma was suppressed by use of Ni-filters (thickness 40 μm). In addition, filtering by at total of 1000 μm of Teflon (C_2F_2) was required to sufficiently suppress the strong self-emission of the heated wire. The resulting x-ray image was recorded on an imaging plate detector above the target. The arrival time of the "backlighter pulse" relative to the "heater pulse" could be chosen between 0 and 3 ns.

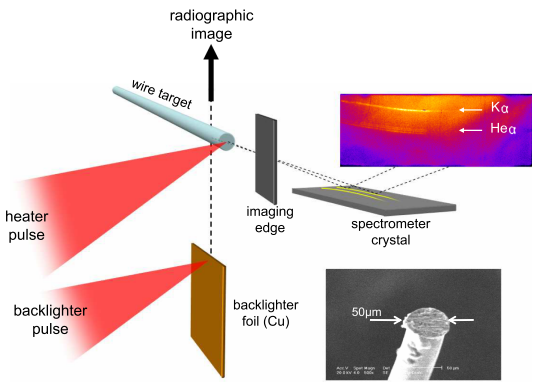

FIG. 1. Experimental setup (see text). The insets show the electron microscope image of the polished wire tip and the x-ray emission spectrum along the wire.

K-shell fluorescence of the titanium wire is viewed side-on with a crystal spectrometer. Spatial resolution along the wire axis is achieved by placing a Ni-foil (thickness 25 μm) at a distance of 4.3 mm from the target between target and spectrometer crystal. The edge of the Ni-foil is oriented perpendicular to the wire axis and limits the length of the wire seen by the spectrometer depending on the position along the non-dispersive direction on the detector. Thus, the measured intensity profile represents the wire emission integrated spatially along the wire axis, the actual distribution is obtained from the local slope of the signal. Spatial resolution is limited by the 0.8° mosaic spread of the employed highly oriented pyrolytic graphite crystal to approximately 25 μm. The spectrometer covers a spectral range of <4.5 keV to 4.8 keV with a spectral resolution of 11 eV. A typical spectrum from the laser-irradiated wires (Fig. 1 inset) shows the Ti-K_α-line (at 4.51 keV) extending more than 200 μm into the wire. Besides the K_α-line, we observe the He-like resonance (at 4.75 keV) and intercombination line rising sharply at the wire tip, indicating a thin (<25 μm) plasma at keV temperatures, which we attribute to the laser absorption region within the blow-off plasma. Satellite-emission arising from Ti-ions with a partially ionized L-shell (Ti^{12+} and higher) is not observed.

The wide spectral acceptance of the spectrometer enables us to determine the number of K_α-photons emitted along the wire without the need to model target heating and spectral shifts as necessary when using narrow-band crystal imagers.[21,22] The spectrometer response was cross-calibrated against an x-ray CCD working in single-photon mode, which in turn had been absolutely calibrated using a radioactive source. We estimate the error of this absolute calibration to be of order 10%. Local variations of the crystal reflectivity were corrected for with a dedicated flat-fielding shot on a Titanium foil with the imaging Ni-foil removed. Fig. 3 shows the measured K_α line-emission integrated along the wire. The measurement points are obtained as the amplitude of a Gaussian fit function through a lineout of width 25 μm (corresponding to the spatial resolution), and the error indicated is the uncertainty in the fit parameter, combined with the error from the flat-fielding shot. We find that a total of 2×10^{13} photons is emitted over the full length of the wire. Emission is strongest at the wire tip, rapidly decreasing to 10% after approximately 210 μm.

III. DETERMINATION OF ENERGY DEPOSITION

Measurement of the absolute K_α-yield spatially resolved along the wire enables us to directly determine the collisional energy deposition within the target, without the need to rely on extensive numerical modeling of the hot-electron generation and transport. K_α-generation is computed using cross-sections from the relativistic binary encounter Bethe model for K-shell ionization[23] and the fluorescence yield of 0.214 for Ti.[24] For slowing down of the electrons in the wire and energy exchange with the target, we used stopping powers obtained from the ESTAR database.[25] Fig. 2 shows both $\sigma_K(E)$ and $(dE/dx)_{coll.}$. We find that the ratio, and consequently also the ratio of energy loss per emitted number of K-alpha photons, dE/dK_α is approximately constant over most of the hot electron energies relevant in the experiment. Thus, it is intuitively clear that the amount of K-shell fluorescence is to a good approximation directly proportional to the collisional energy deposition. We calculate the K_α-emission along the wire assuming a source of hot electrons at the tip of the wire. Re-absorption of the K_α-signal within the wire is accounted for using tabulated cold opacities. The electrons are slowed down using collisional stopping powers, and the model assumes that the electrons are confined to the wire volume due to refluxing. We find that a 2-temperature electron distribution function,

$$f(E) = \frac{N_1}{k_B T_1}\exp\left[-\frac{E}{k_B T_1}\right] + \frac{N_2}{k_B T_2}\exp\left[-\frac{E}{k_B T_2}\right], \quad (1)$$

where the hot-electron temperatures $T_{1,2}$ and the number of hot electrons $N_{1,2}$ are the only free fitting parameters, matches well the observed K_α-profiles. The best fit of the model to the data in Fig. 3 ensues $N_1 = 2.9 \times 10^{14}$ and a hot electron temperature of $T_1 = 110$ keV, which is in good agreement with Beg's scaling[26] for the peak laser intensities employed in this experiment. This corresponds to a fraction $\epsilon_1 = N_1 k_B T_1 / E_{laser} = 14\%$ of the laser energy converted to hot electrons with temperature T_1. The fit is strongly sensitive to the parameters T_1 and ϵ_1 with fitting errors of $\pm 15\%$ and $\pm 10\%$, respectively (see Fig. 3 for $T_1 \pm 20$ keV). For the hotter electron component, the data impose limits of $T_2 \geq 400$ keV and $\epsilon_2 \leq 1.6\%$. After adjusting the electron spectrum to fit the measured K_α-distribution, the model yields the energy deposited in the target by the hot electrons due to collisional energy loss.

To ensure that collisional energy deposition dominates the total heating, we estimate resistive heating of the target caused by the return current drawn within the wire to balance the intense forward hot electron current. As the bulk electron density is several orders of magnitude larger than the hot electron density, the average velocities of electrons constituting the return current are slow and do not excite K_α. Therefore, this type of energy deposition cannot be seen by the K_α-spectrometer. We calculate heating due to return currents within the "rigid beam" model.[27] The increase in internal energy U of the bulk target due to resistive heating is computed by $(dU/dt)_{res.} = \eta j^2$, where the return current density is $j = -j_{hot} = (dQ/dt)/A$ over the wire cross section A. The hot electron current dQ/dt is assumed to follow the laser pulse shape with the total charge $\int (dQ/dt)dt$ obtained directly from the measured K_α yields. The resistivity is calculated using the Drude model as $\eta = m\nu_{ei}/(n_e e^2)$, where e and m are electron charge and mass, respectively. The electron density is $n_e = \bar{Z} n_i$, and for the short time-scale, we can assume constant ion density n_i corresponding to the target at solid density. The average charge state $\bar{Z}$ is temperature dependent (due to thermal ionization) and is calculated using the collisional-radiative atomic kinetics code FLYCHK.[28] The collision frequency is calculated by $1/\nu_{ei} = 1/\nu_{max} + 1/\nu_{sp}$, where $\nu_{max} = v_{th}/d_{ii}$ is the maximum collision frequency of electrons at thermal velocity v_{th} with mean free path of the average ion-ion distance

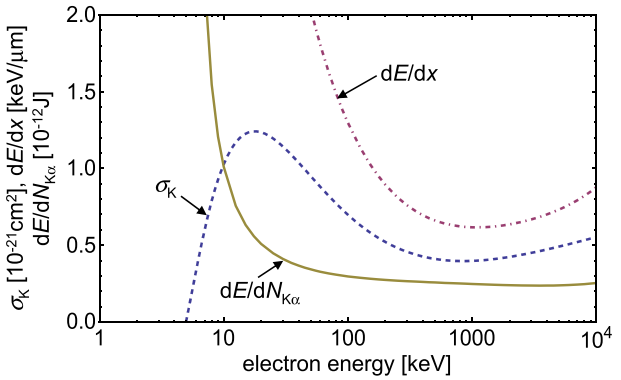

FIG. 2. Cross section for K-shell ionization and collisional stopping power. The ratio of energy loss to K-shell ionization is approximately constant for electron energies >20 keV.

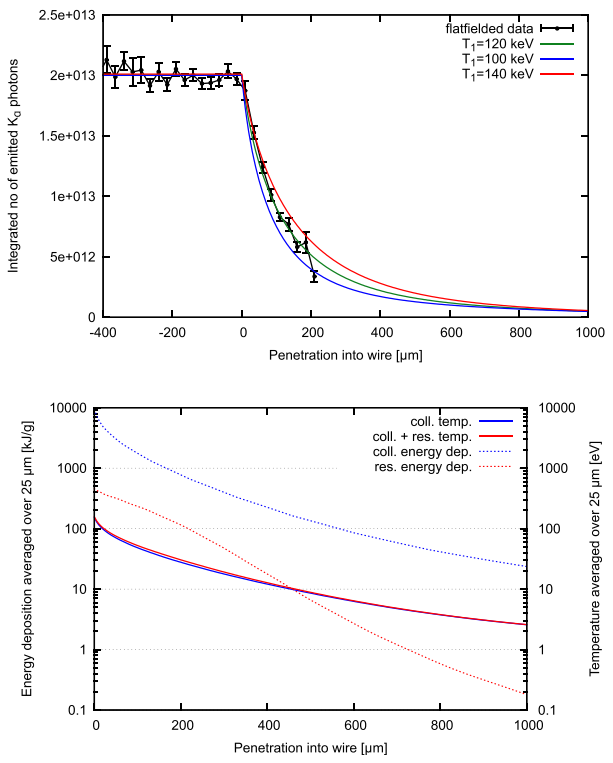

FIG. 3. (Top) Measured K_α-emission along the titanium wire (in the region <0 the entire wire is seen by the spectrometer). The fit to the data yields the hot electron distribution at the wire tip. (Bottom) Energy deposition (collisional and resistive), and resulting target temperatures, as inferred from the K_α-emission.

$d_{ii} = (\frac{4}{3}\pi n_i)^{-1/3}$, and ν_{sp} is the classical Spitzer limit for high temperatures.

Fig. 3 shows both the collisional and resistive energy deposition along the wire. In contrast to hot electron transport studies in thin wire targets attached to gold cones or to a "nail-head," which suggested strong ohmic inhibition due to the enormous currents at intensities exceeding 10^{20} W/cm^2,[18,22,29] we find at the low intensities employed in this experiment that resistive heating only contributes a small fraction (≈5%) to the total energy deposition. This can be regarded as an upper limit since slowing down of the hot electrons by the self-generated fields is neglected in the rigid beam approximation. We thus expect the target heating to be dominated by collisions, which we have accurately inferred from the K_α-emission along the wire.

The target bulk temperature reached after the hot electron fraction has slowed down completely (6 ps after their generation) is determined by use of the PROPACEOS equation of state[30] and is also shown in Fig. 3. We find temperatures ranging from >150 eV at the tip of the wire, to ~30 eV at a depth of 200 μm into the wire, and further to ~5 eV at 700 μm. The maximum temperature of 150 eV is consistent with the upper limit imposed by the absence of satellite-emission from Ti-ions with a partially ionized L-shell in the K-shell emission spectra.

IV. ANALYSIS OF RADIOGRAPHIC MEASUREMENTS, HYDRODYNAMIC MODELING

The signal generated in the image plate by the x-ray photons from the backlighter can be written as

$$S(\rho_A) = \int N_{ph}(E) R_{det}(E) T_{Filter}(E) \exp[\rho_A \mu_m(E)] dE. \quad (2)$$

Here, $N_{ph}(E)$ is the number of x-ray photons of energy E per energy interval dE, emitted into the solid angle subtended by one pixel of the detector. The response of the detector is $R_{det}(E)$, i.e., the number of counts produced per incident photon at energy E, and $T_{Filter}(E)$ accounts for the energy dependent transmission of the filters in front of the detector. Material in the path from the backlighter to a detector pixel causes attenuation of the x-ray flux by $\exp(\rho_A \mu_m(E))$, where $\mu_m(E)$ is the mass attenuation coefficient (units [cm^2/g]). The areal mass density $\rho_A = \int \rho(y) dy$ is the mass density integrated along the path of the x-rays to the detector (here along the y-direction), and, consequently, the attenuation of the signal is a measure of ρ_A.

In the case of a backlighter source emitting over a wide energy range, as is the case in our experiment, the dependence of the total signal on ρ_A through Eq. (2) is non-trivial and in principle would require accurate knowledge of all the energy dependent quantities. Direct calibration by placing samples of the target material of various (known) thicknesses over the detector, as, e.g., used in Ref. 31, cannot be applied here, since the target itself, being heated by intense hot electron currents, is a strong source of hard x-ray bremsstrahlung emission, which will distort the calibration. However, the situation is simplified when the signal is generated mostly by "hard," highly penetrating photons, where $\rho_A \mu_m(E) \ll 1$. In this case, Eq. (2) can be approximated to $S(\rho_A) \approx S(0) - \rho_A \bar{\mu}$, i.e., the signal attenuation is directly proportional to ρ_A. Here, $S(0)$ is the unattenuated signal, and $\bar{\mu} = \int N_{ph}(E) R_{det}(E) T_{Filter}(E) \mu_m(E) dE$ is the average attenuation coefficient weighted by the signal. Fig. 4(a) shows $\rho_0 d_{wire} \mu_{m,Ti}(E)$, where $\rho_0 = 4.51$ g/cm^2 is the mass density of solid Titanium and $d_{wire} = 50$ μm the initial wire diameter. Consequently, $\rho_0 d_{wire}$ will be the maximum ρ_A expected in this experiment. We find that $\rho_0 d_{wire} \cdot \mu_{m,Ti}(E) < 0.1$ for photon energies >30 keV. Also, Fig. 4(a) shows the transmission $T_{Filter}(E)$ of the filters as used in the experiment and the image plate response. The latter is assumed to be proportional to the energy deposition in the sensitive layer, which is calculated from the properties of the image plate. The filters employed here strongly suppress photons at energies below 10 keV, and the total response is strongest in the photon energy range of 20…100 keV. Determining the accuracy of the linear approximation would require knowledge of the backlighter emission spectrum $N_{ph}(E)$. Here, we have run Monte-Carlo simulations using the code EGSNRC.[32] Electron populations with a 1-temperature distribution and a total energy corresponding to 10% of the backlighter laser energy were injected into a thin copper foil. The electrons are reflected back and forth in the foil until slowed down. Fig. 4(b) shows the resulting x-ray emission for hot electron temperatures of 25…200 keV (according to Beg's scaling, temperatures of 50…100 keV would be expected at the laser intensity on the backlighter target). The insert in Fig. 4(b) shows the result of Eq. (2) for $\rho_A \le \rho_0 d_{wire}$. The maximum predicted backlighter attenuation lies between 10% and 17%, for hot electron temperatures of 25 keV and 200 keV, respectively. In fact, our radiographic images of cold wires, i.e., when only the backlighter

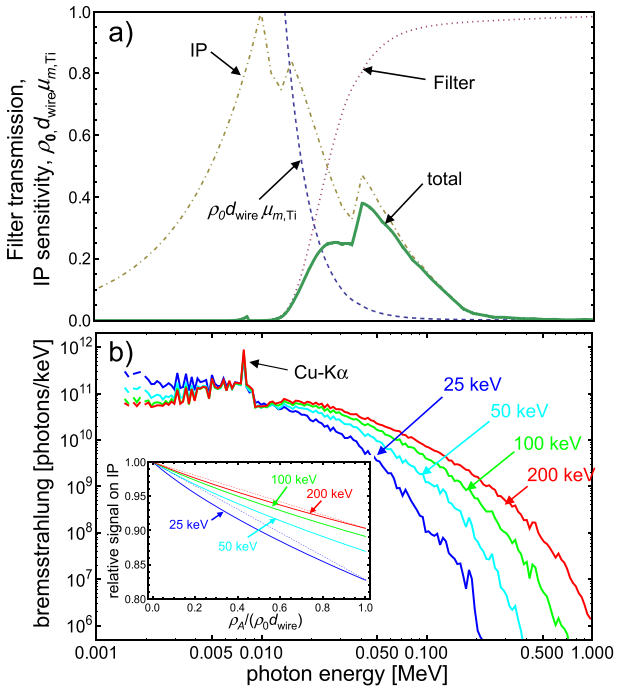

FIG. 4. (a) Filter transmission, image plate response, and $\rho_0 d_{wire} \mu_{m,Ti}$ (see text). (b) Calculated backlighter emission spectra for hot electron temperatures of 25…200 keV. The calculated signal on the image plate (inset) is approximately proportional to the areal density ρ_A.

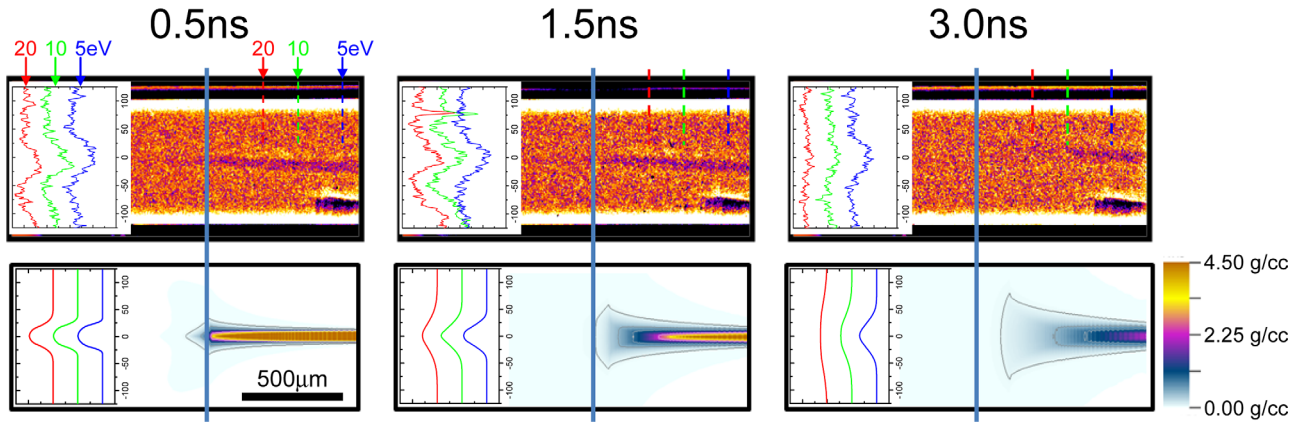

FIG. 5. (Top) X-ray radiographic images taken 0.5, 1.5, and 3 ns after the heater pulse show the expansion of the heated wire target. (Bottom) Radial mass density, obtained from 2D hydrodynamic simulations. The blue lines indicate the position of the wire tip before the shot.

laser was fired, show a maximum backlighter attenuation of order 10%–15%, supporting the assumption of mostly hard photons producing the image. Using the linear approximation with the point at $\rho_0 d_{\text{wire}}$ as reference (dashed lines) will lead to an over-estimation of ρ_A of up to 20% and up to 5% for hot electron temperatures of 25 keV and 200 keV, respectively.

Fig. 5 (top) shows x-ray radiographic images taken at several times up to 3 ns after the target heating. It can be clearly seen that further away from the wire tip the disassembly sets in later, indicating slower expansion of the material at lower temperatures. The wire tip is indicated as well as the positions along the wire where initial temperatures of 20, 10, and 5 eV were reached. The lineouts at these locations show the raw signal on the image plate detector.

We compare the images to radiation-hydrodynamic calculations of the wire expansion. Calculations were performed in 2D axially symmetric geometry with the code RALEF-2D;[33] equation of state, thermal conductivity, and spectral opacities were generated by the THERMOS code.[34] As initial conditions, we used the specific energy density determined from the K_α-emission (Sec. III). According to Ref. 35, the transition temperature to a radiation dominated plasma can be estimated as $T(\text{keV}) = 2.1\rho^{(1/3)}$. At our densities this transition temperature would amount to several keV, at least an order of magnitude higher than the temperatures reached within the wire. Comparison of runs with and without the radiation package indeed showed that radiation transport is negligible and the target evolution can be well described as a isentropic hydrodynamic expansion. Fig. 5 (bottom) shows the calculated radial mass density $\rho(r,z)$ at the times where radiographic images were taken. As expected, further away from the wire tip, where temperatures are lower, the expansion is significantly slower than close to the wire tip. At a depth of 300 μm into the wire where the temperature has dropped to <20 eV, longitudinal temperature gradients are less than 0.05 eV/μm, corresponding to a pressure gradient of $\sim$30 kbar/ μm. Longitudinal displacement of mass elements can be estimated to $(\partial P/\partial x)t^2/(2\rho)$, corresponding to $\sim$3 μm over a duration of $t = 3$ ns (ρ is the mass density). Consequently, we find negligible differences between the 2D-results and calculations in 1D cylindrical geometry when comparing the temporal evolution of mass density at a fixed location along the wire. This effectively means that we can follow the isentropic quasi-1D expansion of HED matter, choosing an initial temperature by the corresponding position along the wire. The lineouts in Fig. 5 (bottom) correspond to the same locations as in the experimental images, i.e., at initial temperatures of 20, 10, and 5 eV, and show the Abel transform $\rho_A(x,z) = 2\int_{r=x}^{\infty} \rho(r)\frac{r}{\sqrt{r^2-x^2}}dr$ projecting the axially symmetric mass density onto the detector plane.

Performing the inverse Abel transform on the data (top) leads to large errors due to the strong noise in the data. Therefore, to allow a more quantitative comparison of radiographic data and hydrodynamic calculations, we show in Fig. 6 the temporal evolution of the areal mass density at the center of the lineout, $\rho_A(x=0)$, for initial temperatures of 20, 10, and 5 eV, respectively. The experimental values were determined as the amplitude of a peak function fitted through the lineout and are normalized to the attenuation at a location far from the wire tip, where we can assume $\rho_A = \rho_0 d_{\text{wire}}$. The error bars arise from the fit uncertainty due to the image noise, and from uncertainties in the shot-to-shot relative positioning of radiographs vs. K_α-spectra, which determines the accuracy in determining the location along the wire. We

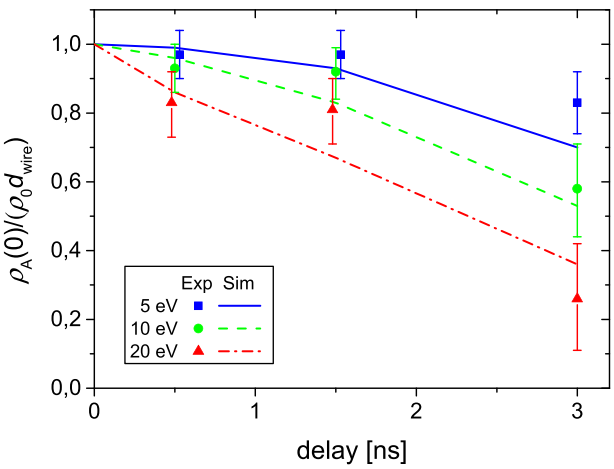

FIG. 6. Temporal evolution of the areal mass density at the center, $\rho_A(0)$, normalized to the initial $\rho_0 d_{\text{wire}}$, for temperatures of 20, 10, and 5 eV, respectively, compared to 1-D hydrodynamic calculations. (The experimental points at 0.5 and 1.5 ns are slightly displaced in time for better visibility.)

find a good agreement between measured and calculated central areal densities over the investigated delay times. Thus, the expansion measurement corroborates the energy deposition as obtained from the K_α-emission and demonstrates heating of the wire target over hundreds of micrometers. On the other hand, having measured the energy deposition, the expansion measurements confirm the EOS used in the hydro-simulations in the accessed parameter regime.

V. CONCLUSION

In conclusion, we have heated titanium wire targets employing hot electrons produced by intense-laser matter interaction. The energy deposition in the target was directly extracted with high precision from spatially resolved K_α-calorimetry. X-ray radiography confirms that the target remains at its initial density over times large compared to the heating time and also shows the subsequent isentropic quasi-1D expansion of the target. This experimental scheme provides large, well defined samples of WDM. It will also provide a controlled path to expansion measurements at lower temperatures (<1 eV) where effects due to explosive boiling are expected when the target passes through metastable states in the two-phase liquid-vapor regime.[36] We note that radiographic measurements using the quasi-monochromatic source spectra obtained at x-ray free electron lasers will readily yield density resolution on the percent level. This would enable direct measurements of pressure-density isentropes as proposed in Ref. 37, allowing stringent tests to EOS models in this challenging parameter regime.

ACKNOWLEDGMENTS

We would like to acknowledge the support by the PHELIX laser team. This work was supported by EMMI.

[1]J. Lindl, Phys. Plasmas **2**, 3933 (1995).
[2]T. Guillot, Science **286**, 72 (1999).
[3]R. Redmer, Phys. Rep. **282**, 35 (1997).
[4]R. W. Lee, S. J. Moon, H.-K. Chung, W. Rozmus, H. A. Baldis, G. Gregori, R. C. Cauble, O. L. Landen, J. S. Wark, A. Ng, S. J. Rose, C. L. Lewis, D. Riley, J.-C. Gauthier, and P. Audebert, J. Opt. Soc. Am. B **20**, 770 (2003).
[5]D. G. Hicks, T. R. Boehly, P. M. Celliers, J. H. Eggert, S. J. Moon, D. D. Meyerhofer, and G. W. Collins, Phys. Rev. B **79**, 014112 (2009).
[6]S. Brygoo, E. Henry, P. Loubeyre, J. Eggert, M. Koenig, B. Loupias, A. Benuzzi-Mounaix, and M. R. Le Gloahec, Nature Mater. **6**, 274 (2007).
[7]P. K. Patel, A. J. Mackinnon, M. H. Key, T. E. Cowan, M. E. Foord, M. Allen, D. F. Price, H. Ruhl, P. T. Springer, and R. Stephens, Phys. Rev. Lett. **91**, 125004 (2003).
[8]G. M. Dyer, A. C. Bernstein, B. I. Cho, J. Osterholz, W. Grigsby, A. Dalton, R. Shepherd, Y. Ping, H. Chen, K. Widmann, and T. Ditmire, Phys. Rev. Lett. **101**, 015002 (2008).
[9]P. M. Nilson, A. A. Solodov, J. F. Myatt, W. Theobald, P. A. Jaanimagi, L. Gao, C. Stoeckl, R. S. Craxton, J. A. Delettrez, B. Yaakobi, J. D. Zuegel, B. E. Kruschwitz, C. Dorrer, J. H. Kelly, K. U. Akli, P. K. Patel, A. J. Mackinnon, R. Betti, T. C. Sangster, and D. D. Meyerhofer, Phys. Rev. Lett. **105**, 235001 (2010).
[10]J. Myatt, W. Theobald, J. A. Delettrez, C. Stoeckl, M. Storm, T. C. Sangster, A. V. Maximov, and R. W. Short, Phys. Plasmas **14**, 056301 (2007).
[11]H.-S. Park, D. M. Chambers, H.-K. Chung, R. J. Clarke, R. Eagleton, E. Giraldez, T. Goldsack, R. Heathcote, N. Izumi, M. H. Key, J. A. King, J. A. Koch, O. L. Landen, A. Nikroo, P. K. Patel, D. F. Price, B. A. Remington, H. F. Robey, R. A. Snavely, D. A. Steinman, R. B. Stephens, C. Stoeckl, M. Storm, M. Tabak, W. Theobald, R. P. J. Town, J. E. Wickersham, and B. B. Zhang, Phys. Plasmas **13**, 056309 (2006).
[12]P. Neumayer, B. Aurand, M. Basko, B. Ecker, P. Gibbon, D. C. Hochhaus, A. Karmakar, E. Kazakov, T. Kühl, C. Labaune, O. Rosmej, An. Tauschwitz, B. Zielbauer, and D. Zimmer, Phys. Plasmas **17**, 103103 (2010).
[13]P. M. Nilson, W. Theobald, J. F. Myatt, C. Stoeckl, M. Storm, J. D. Zuegel, R. Betti, D. D. Meyerhofer, and T. C. Sangster, Phys. Rev. E **79**, 016406 (2009).
[14]G. Gregori, S. B. Hansen, R. Clarke, R. Heathcote, M. H. Key, J. King, R. I. Klein, N. Izumi, A. J. Mackinnon, S. J. Moon, H.-S. Park, J. Pasley, N. Patel, P. K. Patel, B. A. Remington, D. D. Ryutov, R. Shepherd, R. A. Snavely, S. C. Wilks, B. B. Zhang, and S. H. Glenzer, Contrib. Plasma Phys. **45**, 284 (2005).
[15]F. Perez, L. Gremillet, M. Koenig, S. D. Baton, P. Audebert, M. Chahid, C. Rousseaux, M. Drouin, E. Lefebvre, T. Vinci, J. Rassuchine, T. Cowan, S. A. Gaillard, K. A. Flippo, and R. Shepherd, Phys. Rev. Lett. **104**, 085001 (2010).
[16]P. M. Nilson, J. R. Davies, W. Theobald, P. A. Jaanimagi, C. Mileham, R. K. Jungquist, C. Stoeckl, I. A. Begishev, A. A. Solodov, J. F. Myatt, J. D. Zuegel, T. C. Sangster, R. Betti, and D. D. Meyerhofer, Phys. Rev. Lett. **108**, 085002 (2012).
[17]S. D. Baton, M. Koenig, P. Guillou, B. Loupias, A. Benuzzi-Mounaix, J. Fuchs, C. Rousseau, L. Gremillet, D. Batani, A. Morace, M. Nakatsutsumi, R. Kodama, and Y. Aglitskiy, High Energy Density Phys. **3**, 358 (2007).
[18]J. S. Green, K. L. Lancaster, K. U. Akli, C. D. Gregory, F. N. Beg, S. N. Chen, D. Clark, R. R. Freeman, S. Hawkes, C. Hernandez-Gomez, H. Habara, R. Heathcote, D. S. Hey, K. Highbarger, M. H. Key, R. Kodama, K. Krushelnick, I. Musgrave, H. Nakamura, M. Nakatsutsumi, N. Patel, R. Stephens, M. Storm, M. Tampo, W. Theobald, L. Van Woerkom, R. L. Weber, M. S. Wei, N. C. Woolsey, and P. A. Norreys, Nat. Phys. **3**, 853 (2007).
[19]V. Bagnoud, B. Aurand, A. Blazevic, S. Borneis, C. Bruske, B. Ecker, U. Eisenbarth, J. Fils, A. Frank, E. Gaul, S. Goette, C. Haefner, T. Hahn, K. Harres, H.-M. Heuck, D. Hochhaus, D. H. H. Hoffmann, D. Javorková, H.-J. Kluge, T. Kuehl, S. Kunzer, M. Kreutz, T. Merz-Mantwill, P. Neumayer, E. Onkels, D. Reemts, O. Rosmej, M. Roth, T. Stoehlker, A. Tauschwitz, B. Zielbauer, D. Zimmer, and K. Witte, Appl. Phys. B **100**, 137 (2010).
[20]H.-S. Park, B. R. Maddox, E. Giraldez, S. P. Hatchett, L. T. Hudson, N. Izumi, M. H. Key, S. Le Pape, A. J. MacKinnon, A. G. MacPhee, P. K. Patel, T. W. Phillips, B. A. Remington, J. F. Seely, R. Tommasini, R. Town, J. Workman, and E. Brambrink, Phys. Plasmas **15**, 072705 (2008).
[21]K. U. Akli, M. H. Key, H. K. Chung, S. B. Hansen, R. R. Freeman, M. H. Chen, G. Gregori, S. Hatchett, D. Hey, N. Izumi, J. King, J. Kuba, P. Norreys, A. J. Mackinnon, C. D. Murphy, R. Snavely, R. B. Stephens, C. Stoeckel, W. Theobald, and B. Zhang, Phys. Plasmas **14**, 023102 (2007).
[22]T. Ma, H. Sawada, P. K. Patel, C. D. Chen, L. Divol, D. P. Higginson, A. J. Kemp, M. H. Key, D. J. Larson, S. Le Pape, A. Link, A. G. MacPhee, H. S. McLean, Y. Ping, R. B. Stephens, S. C. Wilks, and F. N. Beg, Phys. Rev. Lett. **108**, 115004 (2012).
[23]Y. Kim, J. Santos, and F. Parente, Phys. Rev. A **62**, 052710 (2000).
[24]M. Krause, J. Phys. Chem. Ref. Data **8**, 307 (1979).
[25]M. J. Berger, J. S. Coursey, M. A. Zucker, and J. Chang, ESTAR, PSTAR, and ASTAR: Computer Programs for Calculating Stopping-Power and Range Tables for Electrons, Protons, and Helium Ions (version 1.2.3), National Institute of Standards and Technology, Gaithersburg, MD.
[26]F. N. Beg, A. R. Bell, A. E. Dangor, C. N. Danson, A. P. Fews, M. E. Glinsky, B. A. Hammel, P. Lee, P. A. Norreys, and M. Tatarakis, Phys. Plasmas **4**, 447 (1997).
[27]J. R. Davies, Phys. Rev. E **65**, 026407 (2002).
[28]H.-K. Chung, M. H. Chen, W. L. Morgan, Y. Ralchenko, and R. W. Lee, High Energy Density Phys. **1**, 3 (2005).
[29]T. Ma, M. H. Key, R. J. Mason, K. U. Akli, R. L. Daskalova, R. R. Freeman, J. S. Green, K. Highbarger, P. A. Jaanimagi, J. A. King, K. L. Lancaster, S. P. Hatchett, A. J. Mackinnon, A. G. MacPhee, P. A. Norreys, P. K. Patel, R. B. Stephens, W. Theobald, L. D. Van Woerkom, M. S. Wei, S. C. Wilks, and F. N. Beg, Phys. Plasmas **16**, 112702 (2009).
[30]J. MacFarlane, I. Golovkin, and P. R. Woodruff, J. Quant. Spectrosc. Radiat. Transf. **99**, 381 (2006).
[31]E. Brambrink, H. G. Wei, B. Barbrel, P. Audebert, A. Benuzzi-Mounaix, T. Boehly, T. Endo, C. D. Gregory, T. Kimura, R. Kodama, N. Ozaki, H.-S. Park, and M. Koenig, Phys. Rev. E **80**, 056407 (2009).

[32]I. Kawrakow and D. W. O. Rogers, "The EGSnrc Code System: Monte Carlo Simulation of Electron and Photon Transport," NRCC Report No. PIRS-701, 2006, Available at http://www.irs.inms.nrc.ca/inms/irs/EGSnrc/EGSnrc.html.
[33]M. M. Basko, J. Maruhn, and An. Tauschwitz, GSI Rep. **2010-1**, 410 (2010).
[34]A. Nikiforov, V. Novikov, and V. Uvarov, *Quantumstatistical Models of Hot Dense Matter: Methods for Computation of Opacity and Equation of State* (Birkhäuser, 2005).
[35]R. P. Drake, *High Energy Density Physics: Fundamentals, Inertial Fusion and Experimental Astrophysics* (Springer Verlag, Berlin, 2006).
[36]V. V. Zhakhovsky, S. A. Pikuz, S. I. Tkachenko, P. V. Sasorov, T. A. Shelkovenko, P. F. Knapp, C. C. Saylor, and D. A. Hammer, in *17th APS SCCM Chicago* (2012), Vol. 1426, pp. 10–13.
[37]M. E. Foord, D. B. Reisman, and P. T. Springer, Rev. Sci. Instrum. **75**, 2586 (2004).